nature cell biology

The bacterial cell division proteins FtsA and FtsZ self-organize into dynamic cytoskeletal patterns

Martin Loose[1,2] and Timothy J. Mitchison[1]

Bacterial cytokinesis is commonly initiated by the Z-ring, a cytoskeletal structure that assembles at the site of division. Its primary component is FtsZ, a tubulin superfamily GTPase, which is recruited to the membrane by the actin-related protein FtsA. Both proteins are required for the formation of the Z-ring, but if and how they influence each other's assembly dynamics is not known. Here, we reconstituted FtsA-dependent recruitment of FtsZ polymers to supported membranes, where both proteins self-organize into complex patterns, such as fast-moving filament bundles and chirally rotating rings. Using fluorescence microscopy and biochemical perturbations, we found that these large-scale rearrangements of FtsZ emerge from its polymerization dynamics and a dual, antagonistic role of FtsA: recruitment of FtsZ filaments to the membrane and negative regulation of FtsZ organization. Our findings provide a model for the initial steps of bacterial cell division and illustrate how dynamic polymers can self-organize into large-scale structures.

As in eukaryotic cells, proteins related to actin and tubulin provide the key structural components coordinating cellular functions in bacteria[1,2]. For example, cell division in most bacteria depends on the tubulin-related GTPase FtsZ and the widely conserved actin-related protein FtsA, which form an annular structure at the middle of the cell[3,4]. Purified FtsZ assembles into polar, straight or gently curved protofilaments in the presence of GTP (refs 5–8) and lateral interactions between FtsZ protofilaments can lead to higher-ordered structures, such as tubules, bundles, circles and sheets[5,6]. In most bacteria, FtsZ is recruited to the membrane by FtsA, which binds to the membrane through a carboxy-terminal amphipathic helix[9,10]. Although binding of ATP is required for FtsA to interact with FtsZ, no ATPase activity of FtsA was found[9–12]. In *Escherichia coli* and other Gammaproteobacteria, FtsZ is also recruited to the membrane by the trans-membrane protein ZipA (refs 13–15) and both membrane anchors are required for successful cell division. Although structurally unrelated, FtsA and ZipA bind to the same C-terminal peptide of FtsZ, which is connected to the rest of the protein through a flexible linker[16,17]. Most previous models for Z-ring formation mainly assumed both proteins to be passive membrane anchors for FtsZ (refs 18–20), an idea also followed in reconstitution studies, where the requirement for physiological membrane anchors was circumvented by supplying FtsZ with its own membrane-targeting peptide[21–23]. However, *in vitro* experiments using an FtsA mutant suggested that the membrane anchor can change the properties of FtsZ assemblies[24], raising the question of whether and how ZipA or FtsA might influence the organization of FtsZ filaments into large-scale, dynamic cytoskeletal structures. To probe the mechanism underlying Z-ring assembly, we set out to reconstitute FtsZ polymerization mediated by wild-type FtsA or ZipA on supported lipid bilayers *in vitro*.

RESULTS

FtsZ and FtsA self-organize into a rapidly reorganizing filament network

Earlier attempts to reconstitute FtsA–FtsZ interaction were frustrated by wild-type FtsA being notoriously difficult to purify. Here, we circumvented this problem by using a SUMO-fusion system for overexpression of FtsA followed by removal of the SUMO-tag (ref. 25). We then used total internal reflection fluorescence microscopy to reveal the behaviour of fluorescently labelled proteins on a supported membrane (Supplementary Fig. 1). First, we added FtsZ labelled with Alexa488 together with unlabelled FtsA and ATP to the buffer above the bilayer to a concentration ratio of [FtsZ]:[FtsA] = 3 : 1 to 5:1, corresponding to the one found *in vivo*[26]. Under these conditions, we saw no FtsZ bound to the membrane. Next we added GTP to promote FtsZ polymerization. After a lag time of about 5 min, short FtsZ filaments started to attach to the membrane. These filaments increased in density and then formed dynamic bundles, which self-organized into coherent, motile assemblies (Fig. 1a,b and Supplementary Videos 1 and 2). Dominant features of this large-scale organization were streams of travelling

[1]Department of Systems Biology, Harvard Medical School, 200 Longwood Avenue, Boston, Massachusetts 02115, USA.
[2]Correspondence should be addressed to M.L. (e-mail: martin_loose@hms.harvard.edu)

Received 30 August 2013; accepted 28 October 2013; published online 8 December 2013; DOI: 10.1038/ncb2885

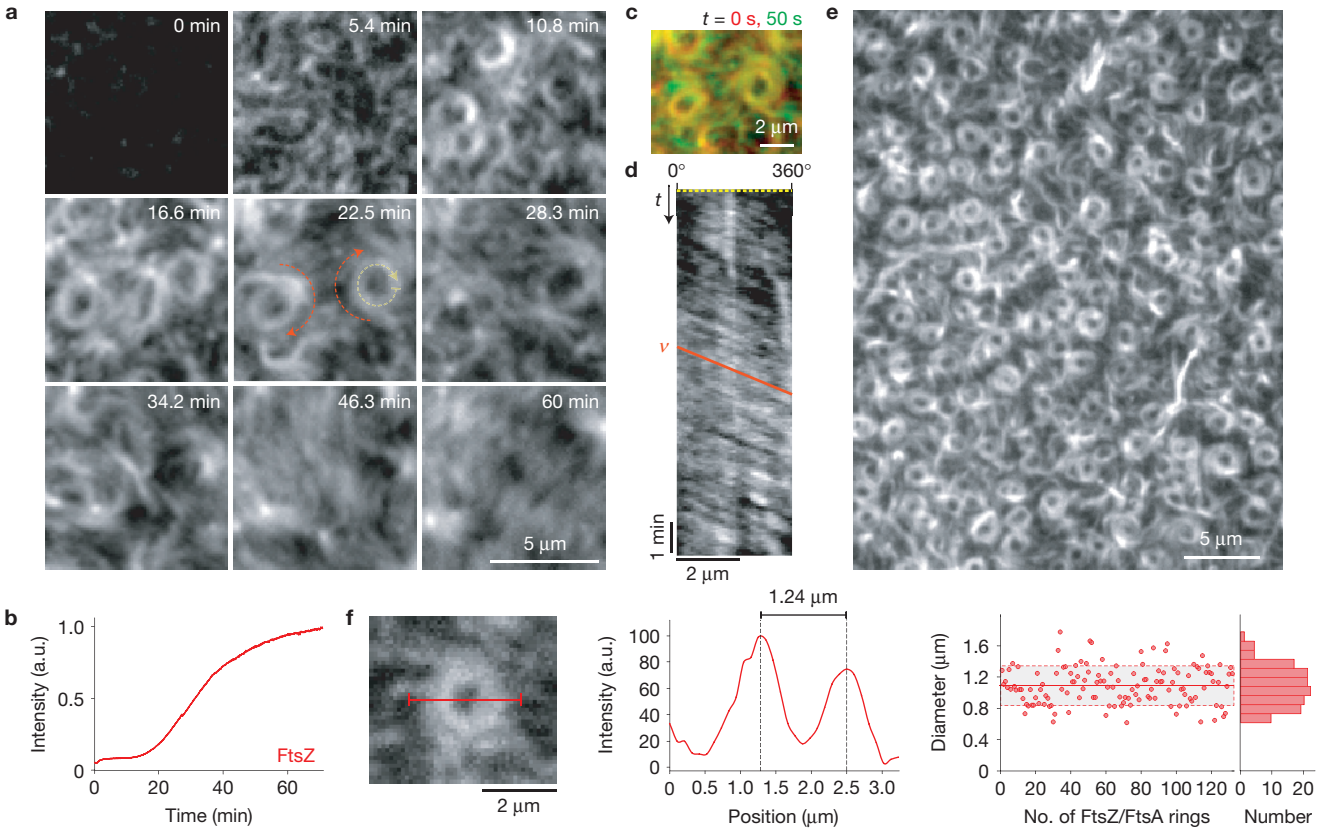

Figure 1 FtsZ and FtsA self-organize into a rapidly reorganizing filament network. (**a**) Snapshots showing typical cytoskeletal patterns of FtsZ emerging from its interaction with FtsA on a supported membrane. Similar results were obtained in more than 100 experiments. After adding GTP (to 3 mM at $t = 0$ min), short filaments of FtsZ start attaching to the membrane. While their density increases, they self-organize into a rapidly reorganizing filament network, forming travelling streams and rotating swirls (orange arrows; FtsZ, 1.5 μM with 10% FtsZ–Alexa488; FtsA, 0.5 μM). (**b**) Representative time–intensity curve corresponding to the amount of FtsZ polymerizing on the membrane after adding GTP. (**c**) Overlay of two individual frames from Supplementary Video 2 separated by 50 s. While FtsZ bundles outside the ring are constantly rearranging, the bundles inside of the vortex are more persistent. (**d**) Representative kymograph along the circumference of a vortex shown in **a**; see yellow dashed arrow at 22.5 min. The slope of the orange line corresponds to the velocity (x/t) of the vortex. Kymographs were obtained and analysed for 40 different vortices. (**e**) Array of dynamic rings of FtsZ. (**f**) Ring diameters were determined by measuring the peak-to-peak distance in the intensity profile (red line shown in micrograph; left). Right, scatter plot of ring diameters (red dots), average value (solid red line, $n = 132$), standard deviation (dashed line and grey background) and corresponding histogram. Source data are given in Supplementary Table 1.

filament bundles, apparently moving in one direction. These streams often formed rotating vortices that persisted for tens of minutes during which their diameter did not change (Fig. 1c). To analyse the rotation of the FtsZ swirls, we generated kymographs along their circumference and found that these rings rotated with a velocity of 6.56 ± 0.69 μm min^{-1} (s.e.m, $n = 40$), corresponding to a radial velocity of 11.47 ± 1.21 degrees s^{-1}, which means that one full rotation required 31.4 ± 3.3 s (Fig. 1d). In some cases a field of vortices covered large areas of the membrane (Fig. 1e and Supplementary Video 3). Although our *in vitro* system did not provide any spatial cues such as membrane curvature or geometric confinement, the FtsZ filaments organized into rings with a similar diameter as the *E. coli* cell (1.09 ± 0.24 μm (s.d., $n = 132$) compared to 0.7–1.4 μm, ref. 27 and Fig. 1f). Furthermore, these vortices were chiral, because all rings rotated clockwise when viewed from the membrane. This dynamic reorganization of FtsZ filaments *in vitro* was reminiscent of the rapidly moving helical pattern during Z-ring assembly seen in *E. coli* cells[28] and *Bacillus subtilis*[29].

The emergence of complex dynamic patterns of FtsZ depended on the presence of both ATP and GTP. When GTP, but no ATP was added, we observed only transient recruitment of FtsZ filaments to the membrane, presumably because some nucleotide from the purification was bound to FtsA (ref. 12). As soon as fresh, exogenous ATP was added, FtsZ reassembled on the membrane (Supplementary Fig. 2a and Video 4). We did not find any ATPase activity of FtsA, and similar dynamic patterns were formed when we substituted ATP with ADP or ATPγS, a non-hydrolysable analogue of ATP, consistent with previous suggestions that FtsA requires nucleotide to interact with FtsZ, but functions without hydrolysing ATP (refs 11,12,30). When we added GMPCPP, a GTP analogue that cannot be hydrolysed by FtsZ, FtsZ formed static bundles of filaments, which did not reorganize over time (Supplementary Video 5). Furthermore, to test the role of FtsA self-interaction, we repeated our experiment with mutants of FtsA, which were found to fail to polymerize *in vivo*[10,12,31,32]. With these FtsA mutants, FtsZ assembled into the same dynamic patterns as with wild-type FtsA, indicating that FtsA polymerization does not play a role for the formation of cytoskeletal patterns (Supplementary Fig. 2b).

To conclude, although GTP and ATP were required for FtsZ–FtsA self-organization, the energy that drives the dynamics of their filament pattern originates solely from GTP hydrolysis coupled to FtsZ polymerization.

The FtsZ filament network reorganizes through FtsZ polymerization dynamics

Next, we were interested in how the dynamics of these cytoskeletal patterns of FtsZ and the directionality of their movement arise. Two models for the remodelling of the Z-ring during cell septum constriction have been proposed[33–35]: First, FtsZ filaments could slide along each other. In this case, single FtsZ subunits would move together with the filament network. Second, FtsZ filaments could reorganize by polymerization dynamics, in which case single FtsZ subunits would remain static. To visualize individual FtsZ molecule dynamics in our *in vitro* experiment, we added small amounts of FtsZ labelled with Cy5 to a background of FtsZ labelled with Alexa488. We found that while the filament network was continuously moving and rearranging, single FtsZ subunits appeared and remained at the same position (Fig. 2a,b and Supplementary Videos 6–8). This observation rules out a sliding mechanism and supports network reorganization by polymerization dynamics, most likely treadmilling. When we analysed the lifetime of FtsZ monomers using single-particle tracking, we found an exponential lifetime distribution corresponding to a first-order reaction with an average lifetime of 7.16 ± 1.23 s (s.d., $n = 24$ analysed videos from five independent experiments with more than 1,500 particles in total; Fig. 2c). This exponential distribution is consistent with the observation that monomer exchange is not limited to the filament ends[36], but can occur along the whole filament[37–39].

When we lowered the concentrations of FtsA and FtsZ, we could observe short individual filaments on the membrane, which often appeared as diffraction-limited spots. Those filaments that were dynamic did not simply diffuse on the membrane; instead we found them to show different kinds of polymerization dynamics. We analysed the behaviour of individual, isolated filaments and found that most of them polymerized from one end and then started to depolymerize from the opposite end at a faster rate ($1.89 \pm 0.48\,\mu m\,min^{-1}$ and $3.97 \pm 1.07\,\mu m\,min^{-1}$, s.d, $n = 18$ from five independent experiments, $P < 0.0001$; Fig. 2d,e and Supplementary Fig. 3 and Video 9). In other cases, both rates were similar and as a result, the polymer traveled across the membrane at a constant length, that is, showing treadmilling dynamics (2.58 ± 0.64 and $2.61 \pm 0.67\,\mu m\,min^{-1}$, s.d, $n = 16$, $P = 0.8978$). Alternatively, filaments appeared to break into shorter fragments before detaching from the membrane (4 out of 38 analysed filaments). Fragmentation of FtsZ filaments supports the idea that FtsZ monomers can exchange along the filament, while monopolar elongation and treadmilling of FtsZ filaments explains the directionality of the reorganizing filament network. Importantly, the polymerization rate of single filaments was about three times slower than the rotation velocity of FtsZ rings, suggesting that at higher protein concentrations FtsZ assembles into oligomers before it is incorporated into the cytoskeletal patterns on the membrane. In summary, we propose that the motion of these structures emerges from polymerization dynamics and not from a sliding mechanism.

Large-scale dynamics emerge from the interaction of FtsZ with FtsA

The observed dynamic patterns could either be an intrinsic property of FtsZ polymerization that simply require the filaments to be attached to a membrane, or they could emerge from a more complex interaction with FtsA. To discriminate between these two possibilities, we first tested a hybrid version of FtsZ that binds autonomously to the membrane through an amphipathic helix at its C terminus[21]. We found that this membrane-targeted FtsZ formed a network of filament bundles on the membrane; however, these bundles were stationary, and did not show large-scale reorganization or dynamic vortices (Supplementary Video 10). Next, we replaced FtsA with ZipA, the alternative membrane anchor of FtsZ. For these experiments, we substituted the trans-membrane domain of ZipA with a His-tag, which was shown to have no role in FtsZ binding[40,41]. This allowed us to attach the rest of the protein to a bilayer containing Ni-chelating lipids, thereby mimicking the permanent membrane attachment of full-length ZipA (ref. 42). As in our experiments with FtsA, we first incubated the membrane with both proteins and then initiated FtsZ polymerization by adding GTP. We found the fluorescent signal of FtsZ to increase homogeneously on these membranes, that is, we did not observe individual filaments starting to bind to the membrane, and a much shorter lag time than in the case of FtsA (Fig. 3a,b and Supplementary Fig. 4). After ~10 min, FtsZ started to condense into long bundles of filaments, in agreement with the observation that ZipA can bundle FtsZ filaments in solution[40]. Although these FtsZ bundles did not show large-scale reorganizations, single-molecule experiments confirmed that these filaments were still dynamic, with a slightly longer average monomer lifetime (Supplementary Fig. 5a). In agreement with this observation, the GTPase rate of FtsZ did not change in the presence of either membrane anchor (Supplementary Fig. 5b).

Together, these results show that the rapidly reorganizing patterns we observed with FtsZ and FtsA emerged from the co-assembly of these two proteins on the membrane and were not the result of intrinsic FtsZ polymerization dynamics.

To investigate the difference between the two membrane anchors, we tested under which conditions ZipA or FtsA recruits FtsZ to the membrane. First, we incubated FtsZ and FtsA with multilamellar vesicles, which we could sediment by centrifugation without pelleting FtsZ polymers. With GTP, but in the absence of FtsA, no FtsZ was found in the pellet (Fig. 3c). In the presence of both proteins, GTP and ATP, we found a fraction of FtsA and FtsZ to co-sediment with the vesicles, but most of the two proteins were still in the supernatant, consistent with the formation of highly dynamic filaments that constantly exchange monomers. Without GTP but with FtsA, no FtsZ was recruited to the membrane, suggesting that FtsA preferentially interacts with polymerized FtsZ. When we performed the same experiment with ZipA, we found that FtsZ co-sedimented with ZipA-decorated vesicles in the presence of GTP, but also when no GTP was added. Consistent with previous publications[41,43], this result shows that in contrast to FtsA, ZipA can also recruit FtsZ monomers to the membrane.

These data can explain why the filament network assembled starting with small FtsZ filaments attaching to the membrane when we used FtsA as a membrane anchor. In the case of ZipA, however, the fluorescence increased homogeneously because FtsZ monomers already on the membrane initiate FtsZ polymerization.

FtsZ and FtsA co-assemble on the membrane

In contrast to ZipA, FtsA can reversibly bind to the membrane. Therefore, we were interested in how FtsA membrane binding relates to FtsZ filament recruitment. To probe this relationship, we repeated our self-organization experiment with both FtsZ and FtsA fluorescently

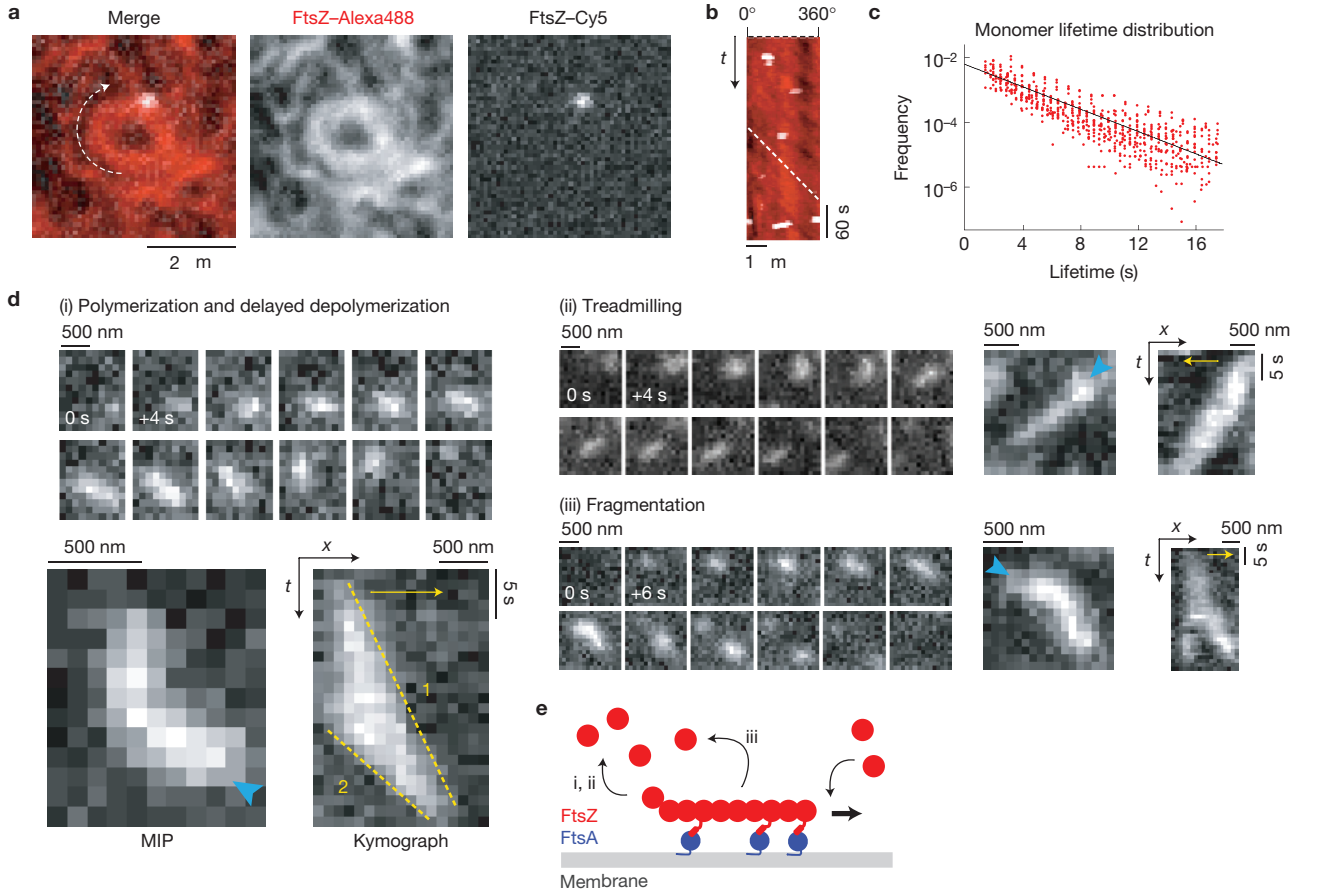

Figure 2 Reorganization of the FtsZ filament network emerges from FtsZ polymerization dynamics and not from filament sliding. (**a**) Typical micrograph of a single FtsZ molecule (white, FtsZ–Cy5) in an FtsZ vortex (red, FtsZ–Alexa488; FtsZ, 1.25 μM with 30% FtsZ–Alexa488 and 0.4% FtsZ–Cy5; FtsA, 0.4 μM). (**b**) Kymograph along the circumference of the vortex shown in **a**. The slope of the white dashed line corresponds to the velocity of the vortex. While the FtsZ ring is rotating, individual FtsZ proteins appear for one to three frames (3–9 s) without moving (Supplementary Videos 6–8). Similar results were obtained in more than 20 experiments. (**c**) Distribution of individual FtsZ lifetimes (red circles) in a linear-log plot and linear fit (black line). See text for details. (**d**) FtsZ filaments can show different kinds of polymerization dynamics when recruited to the membrane by FtsA. Representative snapshots, maximum intensity projections (MIP) and kymographs of (i) filament polymerization and delayed depolymerization, (ii) treadmilling and (iii) fragmentation. Blue arrowheads in MIPs indicate the start of FtsZ polymerization on the membrane; yellow arrows indicate the direction of polymerization. The slopes of the yellow dashed lines correspond to the polymerization (1) and depolymerization rate (2) of the FtsZ filament. (38 filaments from five independent experiments were analysed, see also Supplementary Fig. 3.) (FtsZ, 0.4 μM with 10% FtsZ–Alexa488; FtsA, 0.2 μM.) (**e**) Illustration of a FtsZ filament recruited to the membrane by FtsA. After binding and unipolar polymerization, the filament detaches either after polymerization from the opposite end (i,ii) or after fragmentation (iii).

labelled. Before adding GTP to initiate FtsZ polymerization, the intensity corresponding to both proteins on the membrane was low. After addition of GTP, the fluorescence intensity of FtsA increased diffusely just before FtsZ filaments started to assemble simultaneously with FtsA on the membrane (Fig. 4a,b). Subsequently, the intensity of both proteins increased with similar rates while a dynamic network containing both FtsA and FtsZ assembled on the membrane. FtsZ and FtsA showed synchronized behaviour in motile bundles and rotating vortices (Supplementary Video 12) and on the single-filament level (Supplementary Video 13).

The synchronous assembly of FtsA and FtsZ after we initiated FtsZ polymerization suggested a mutually enhancing interaction between the two proteins. To probe this hypothesis, we initiated the experiment with a low FtsZ concentration, retaining a high concentration of FtsA (Fig. 4c and Supplementary Video 14). Under these conditions, we saw a slow, linear increase of FtsA intensity and short FtsZ filaments transiently binding to the membrane. We then rapidly added FtsZ to a concentration that supports FtsZ filament network formation. Right after the increase in FtsZ, its intensity peaked as short FtsZ filaments covered the membrane. These filaments partially dissociated and then reattached to organize into a dynamic filament network. Remarkably, at this high FtsZ concentration, the intensity of FtsA increased faster and nonlinearly, showing that binding to polymerized FtsZ facilitates membrane-attachment of FtsA during initiation of the cytoskeletal pattern and in equilibrium (Fig. 4d and Supplementary Fig. 7b).

Next, we examined whether the different effects of FtsA and ZipA on FtsZ polymerization could be due to FtsA being able to bind to the membrane reversibly. Therefore, we replaced the C-terminal amphiphatic helix of FtsA with a His-tag and attached FtsA to a membrane containing Ni-chelating lipids as for ZipA. With this permanently attached FtsA, we found FtsZ to form the same dynamic cytoskeletal patterns as with wild-type FtsA (Supplementary Video 15).

These findings show that the formation of a dynamic FtsZ filament network does not depend on the reversible attachment of its membrane

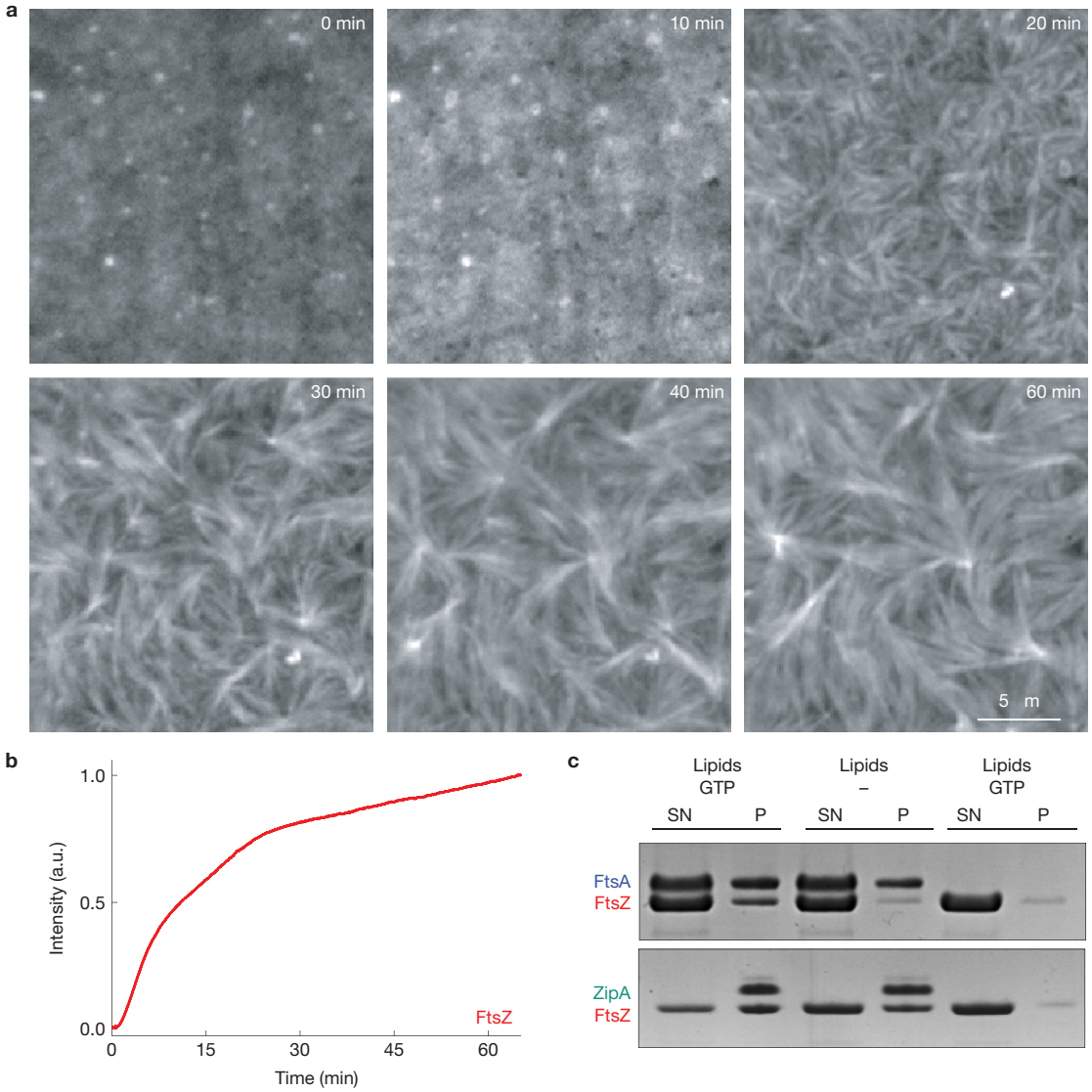

Figure 3 FtsZ organizes into static bundles of dynamic filaments with ZipA as a membrane anchor. (**a**) Representative snapshots showing formation of FtsZ bundles with ZipA as a membrane anchor. Similar results were obtained in more than 70 experiments. First, FtsZ intensity increases homogeneously, followed by condensation of FtsZ into long thick filament bundles (FtsZ, 1.5 μM with 30% FtsZ–Alexa488; His–Δ22-ZipA, 0.5 μM; supported membrane contained 2% Ni-chelating lipids). Different concentrations of Ni-chelating lipids (1–8%) gave similar results (Supplementary Fig. 4). (**b**) Representative time–intensity curve corresponding to the amount of FtsZ bound to the membrane. (**c**) SDS–PAGE gel from a co-pelleting assay with either FtsA and ATP (top row), ZipA (bottom row) or without membrane anchor (far right lanes). In contrast to ZipA, FtsA recruits FtsZ to the membrane only in the presence of GTP (left lanes versus middle lanes); SN, supernatant; P, pellet. Result shown represents eight independent experiments. Uncropped images of gels are shown in Supplementary Fig. 7.

anchor. However, the mutual dependence between FtsZ and FtsA for membrane targeting could be important to prevent FtsA from binding to the membrane and interacting with downstream targets anywhere outside the Z-ring.

FtsA destabilizes the FtsZ filaments network

The initial peak of FtsZ fluorescence and subsequent decrease (Fig. 4c) was reminiscent of damped oscillations observed in biochemical regulation networks, which are typically a consequence of a delayed negative feedback[44–46]. Overshoots and damped oscillations have been seen for tubulin polymerization under certain conditions[47], but we reasoned that a negative feedback from FtsA to FtsZ might be involved here, because a hypermorphic mutant of FtsA has been found to disassemble FtsZ filaments in solution without increasing GTP hydrolysis rate by FtsZ (ref. 11). To probe the influence of FtsA on FtsZ organization we examined whether FtsA could promote disassembly of pre-polymerized FtsZ filaments. Therefore, we first allowed FtsZ to polymerize in solution and then added FtsA to promote their recruitment to the membrane. Consistent with a delayed negative feedback, we found that after adding FtsA, short FtsZ filaments first appeared on the membrane, but then rapidly shortened and detached. Subsequently, both proteins reattached to self-organize into a dynamic polymer network (Fig. 5a and Supplementary Video 16). When we performed the same experiment with ZipA, we did not observe a disassembly of pre-polymerized FtsZ filaments (Fig. 5b and Supplementary Video 16).

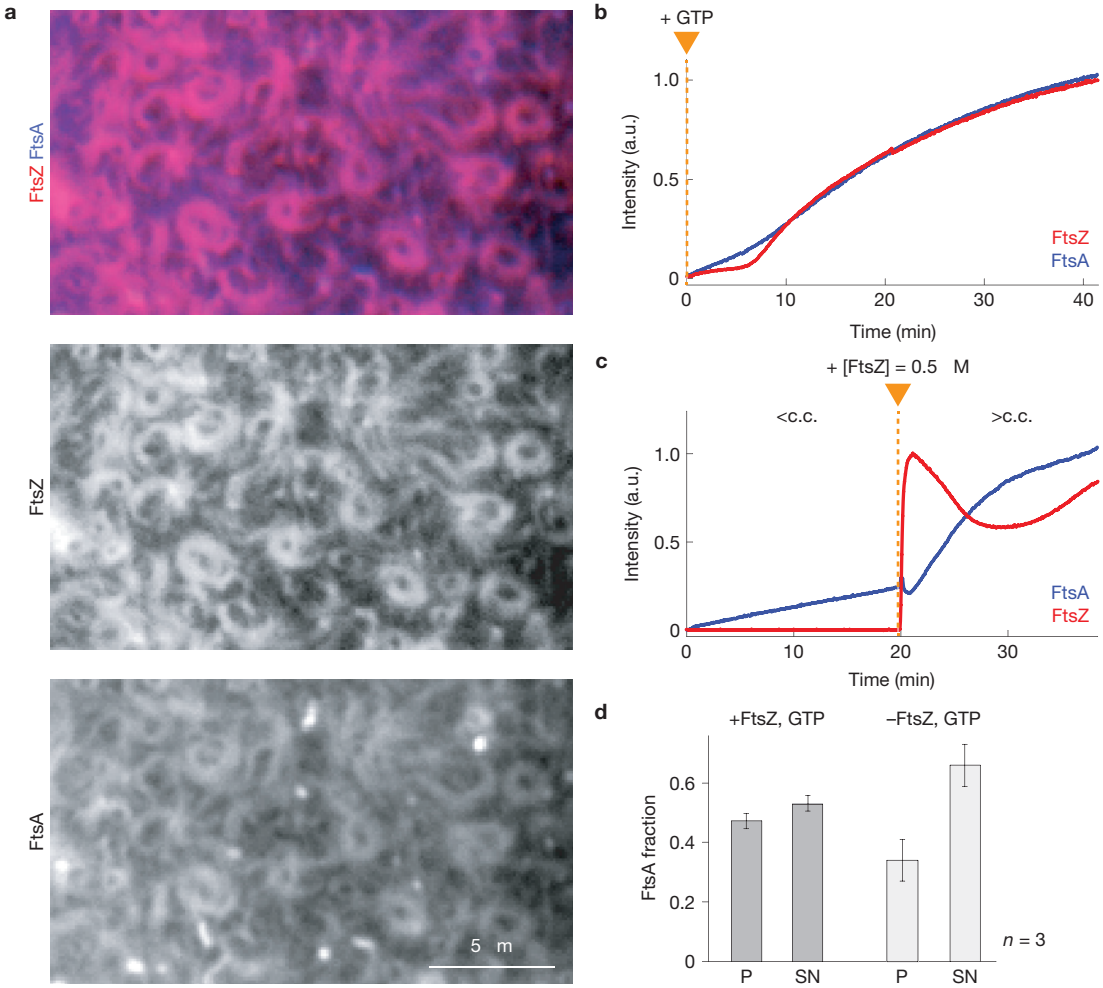

Figure 4 FtsZ and FtsA co-assemble on the membrane. (**a**) Typical micrograph of reorganizing filament patterns with fluorescently labelled FtsZ and FtsA (FtsZ, 1.1 μM with 30% FtsZ–Alexa488; FtsA, 0.4 μM with 10% Cy5–GG-FtsA). (**b**,**c**) Representative intensity traces corresponding to the amount of FtsZ (red) and FtsA (blue). (**b**) After adding GTP (orange arrowhead), FtsZ and FtsA assemble simultaneously on the membrane. Similar micrographs and intensity curves were obtained in more than 50 experiments. (**c**) Binding of FtsA is slow at a low concentration of FtsZ (<c.c., critical concentration of FtsZ allowing for filament network formation), but facilitated at higher FtsZ concentration (>c.c.). The orange triangle indicates time of FtsZ addition. Similar intensity traces were obtained in five independent experiments. (**d**) Bar plot representing the amount of FtsA co-pelleting with vesicles (P) or remaining in the supernatant (SN) after 30 min of incubation (see also Supplementary Fig. 7b). The presence of FtsZ filaments (+FtsZ, GTP) increases the amount of FtsA bound to the membrane ($P = 0.0391$). Error bars represent s.d. from $n = 3$ independent experiments. Source data are given in Supplementary Table 1.

To better compare the effect of FtsA and ZipA on the stability of FtsZ filaments, we performed rapid dilution experiments: at steady state, we diluted the sample five fold to induce disassembly of FtsZ filaments and then determined the rate of decrease in FtsZ fluorescence corresponding to an exponential decay. In the case of FtsA, we could fit the decay curve to a single exponential with a rate of $0.144 \pm 0.06\ s^{-1}$ (s.e.m., $n = 8$). In contrast, with ZipA, we obtained a better fit assuming two separate processes, with a similar and a much slower rate than with FtsA ($0.097 \pm 0.013\ s^{-1}$, $P = 0.5198$, and $0.014 \pm 0.002\ s^{-1}$ s.e.m., $n = 6$, $P = 0.0881$; Fig. 5c). With ZipA, we saw that thick FtsZ bundles could persist on the membrane for more than 5 min, explaining the two rates we obtained from fitting (Fig. 5c and Supplementary Video 17) and a longer residence time for FtsZ on a single-molecule level (Supplementary Fig. 5a). Interestingly, with both membrane anchors present, we found similar, intermediate values for two decay rates and no persisting FtsZ bundles on the membrane (Supplementary Fig. 6).

Finally, in agreement with a negative influence by FtsA, the length and dynamics of FtsZ filaments were strongly influenced by the concentration of FtsA. Using the same concentration for FtsZ (1 μM), we found long, static bundles of filaments at a protein ratio much lower (FtsA, 0.15 μM), but short, highly dynamic filaments at a ratio six times higher than *in vivo* (FtsA, 2 μM; Supplementary Fig. 4b,c).

Together, these data illustrate the ability of FtsA to destabilize FtsZ filaments on the membrane, especially compared with ZipA, allowing for a rapid reorganization of the filament network.

DISCUSSION

In summary, we found that FtsZ and FtsA can self-organize into highly rapidly reorganizing cytoskeletal patterns. We believe that this behaviour emerges from a dual, contradictory influence of FtsA on FtsZ: on the one hand, it enables FtsZ to assemble on the membrane; on the other it provides a negative regulation of FtsZ filament network

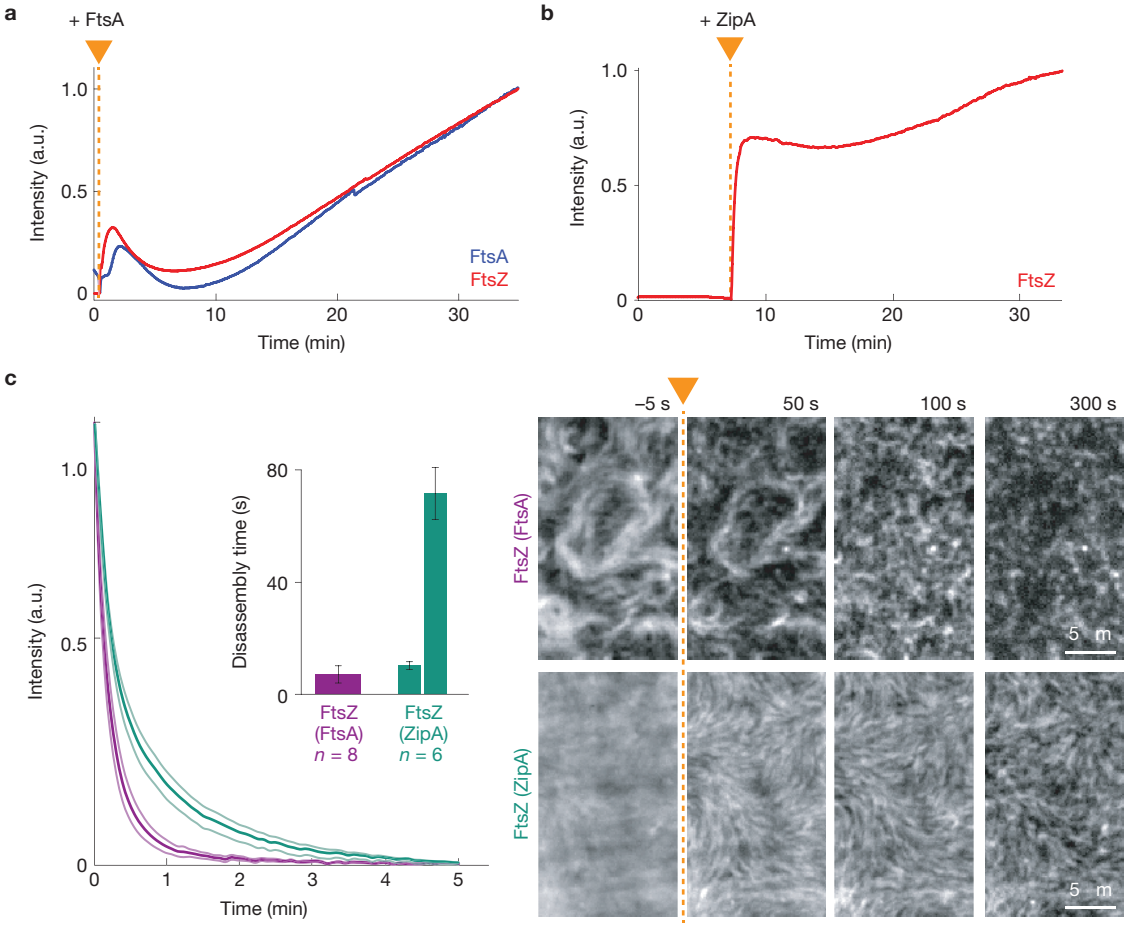

Figure 5 FtsA destabilizes the FtsZ filaments network. (**a**,**b**) Representative intensity traces corresponding to the amount of FtsZ (red) and FtsA (blue) co-assembling on the membrane. Pre-polymerized FtsZ filaments are disassembled after addition of FtsA (**a**), but remain stable after addition of ZipA (**b**; Supplementary Video 16; FtsZ, 1.2 μM; FtsA or His–Δ22-ZipA, 0.3 μM). Intensity traces correspond to four independent experiments respectively. The orange triangle indicates the time of addition of either protein. (**c**) Left: mean intensity traces for FtsZ depolymerization on rapid dilution (FtsZ and FtsA (purple); FtsZ and ZipA (turquoise)). Inset: mean disassembly times obtained from single-exponential (FtsZ with FtsA) and double-exponential fits (FtsZ with ZipA). Thin lines and error bars illustrate s.e.m ($n = 8$ (FtsZ with FtsA) and $n = 6$ (FtsZ with ZipA)). Right: representative snapshots showing dilution-induced FtsZ disassembly. After adding buffer (at the time point indicated by the orange arrowhead and the dashed line), FtsZ filaments rapidly disassembled when recruited by FtsA. In contrast, with ZipA FtsZ bundles can persist for more than 5 min. Intensities of micrographs have been normalized to have constant overall intensity. Raw data are shown in Supplementary Video 17.

organization. Accordingly, the dynamics of this filament network reflect the combination of two interactions superimposed on the intrinsic polymerization dynamics of FtsZ: a fast, mutually positive, bidirectional interaction between FtsA and FtsZ during membrane-binding and a delayed, negative unidirectional feedback from FtsA to FtsZ, which destabilizes the filament network. This negative interaction can explain why with FtsA, FtsZ forms a rapidly reorganizing cytoskeletal pattern. On the basis of our results, we suggest a model of how FtsA and FtsZ self-organize on the membrane (Fig. 6a): FtsA does not recruit FtsZ monomers to the membrane, probably because the binding constant of the C-terminal peptide of FtsZ to FtsA is too weak[12]. An FtsZ-filament–FtsA complex would exhibit multiple bond interactions allowing for attachment to the membrane, where FtsZ filaments can further polymerize. These filaments are highly dynamic, partially because FtsA can cause fragmentation of FtsZ polymers independent of GTP hydrolysis by a yet unknown mechanism. Fragmented filaments might be too short for a strong enough interaction with FtsA, which leads to their detachment from the membrane. With increasing density of short treadmilling filaments on the membrane, lateral interactions, but no filament sliding, give rise to dynamic higher-order structures, such as streams and vortices. The observed chirality of the swirls could be explained by FtsZ filaments being curved[6]. Attachment of curved, polar polymers to a surface through one face automatically creates chiral asymmetries[48] (Fig. 6b). Combined with bundling and treadmilling, these curved dynamic filaments give rise to the rotating rings with a preferred directionality.

In contrast to FtsA, ZipA can also recruit FtsZ monomers to the membrane. One possible explanation for this observation could be that the binding affinity for FtsZ to ZipA is stronger than to FtsA. FtsZ monomers recruited to the membrane can then nucleate the formation of longer filaments, which further organize into thick bundles (Fig. 6c). Filaments in these bundles are dynamic (Supplementary Fig. 5a), but do not show the same large-scale reorganization as with FtsA, because short filaments and even FtsZ monomers remain recruited to the membrane. As a result, FtsZ organizes into static bundles of dynamic filaments with ZipA instead of a rapidly reorganizing filament network.

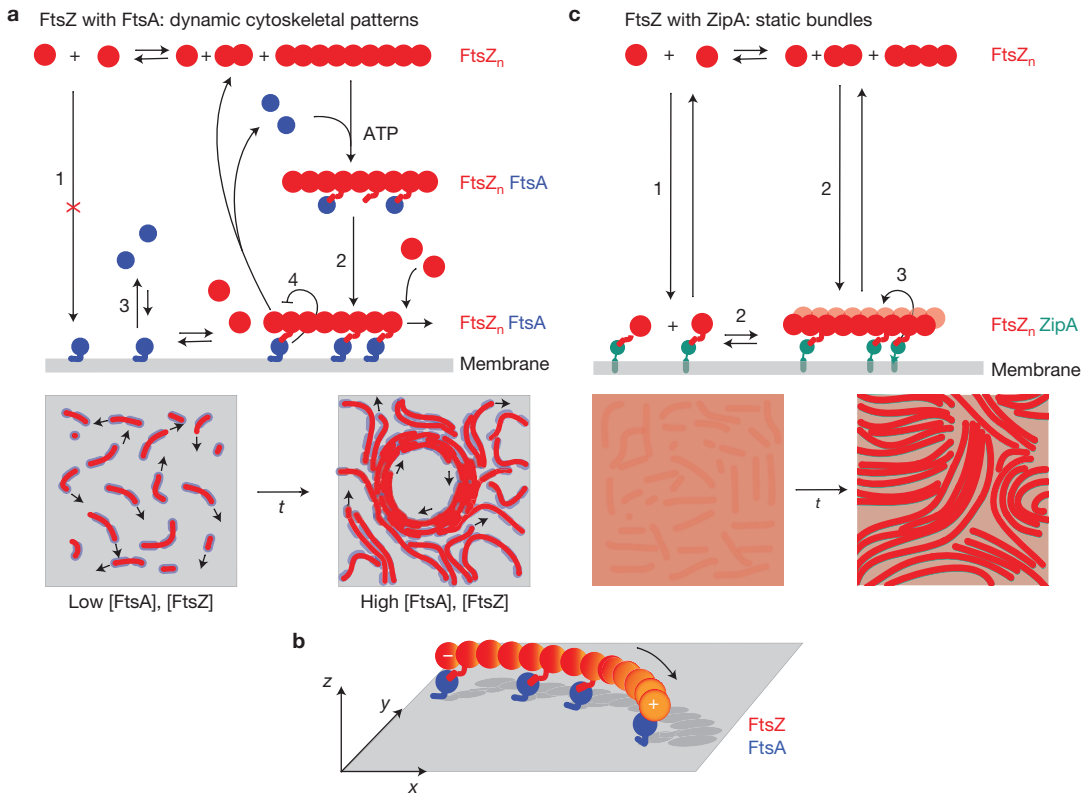

Figure 6 Model for membrane-based FtsZ polymerization. (**a**) Model for FtsZ–FtsA co-assembly on the membrane starting from top left: FtsA does not recruit monomeric FtsZ to the membrane (1). After FtsZ polymerization, an FtsA–FtsZ filament complex forms and attaches to the membrane, which facilitates binding of FtsA to the membrane (2 versus 3). Here, FtsZ filaments can further polymerize or disassemble into short filaments or monomers, which are no longer recruited to the membrane by FtsA, leading to their detachment. The dual, antagonistic role of FtsA is highlighted by two thick arrows: FtsA co-assembles with FtsZ (2), but allows for the rapid disassembly of FtsZ filaments (4). Bottom: with increasing density, lateral interactions between short, dynamic filaments give rise to a rapidly reorganizing filament network, that is, streams and vortices. (**b**) Illustration of a polar, curved FtsZ filament recruited to the membrane by FtsA. Anchoring a polar filament with a curved rigid conformation to a surface creates chiral asymmetries of the system; that is, the membrane-bound filament is not identical to its mirror image. (**c**) Model for the formation of static bundles of dynamic FtsZ filaments mediated by ZipA. In contrast to FtsA, ZipA can recruit polymerized and non-polymerized FtsZ to the membrane (1). Membrane-recruited FtsZ initiates FtsZ polymerization (2). Lateral interactions allow FtsZ filaments to organize into thick bundles, which is further enhanced by ZipA (3). Short filaments and monomeric FtsZ can remain on the membrane after depolymerization of fragmentation. Illustration of GTP hydrolysis by FtsZ has been omitted for clarity.

Self-organized filament patterns have been described for eukaryotic cytoskeletal filaments and molecular motors[49–52]; however, pure solutions of actin filaments or microtubules usually show only nematic ordering and no large-scale rearrangement[53,54]. Dynamic filament patterns in these systems depend on either motor proteins generating shear stress or flow, or multiple other cofactors. Importantly, the FtsA/FtsZ system does not contain any molecular motor that could transform chemical energy into mechanical force to actively move filaments. Instead, on the basis of our finding we favour a model where the large-scale rearrangement of the FtsZ filament network is based on collective polymerization dynamics of FtsZ, which emerge from its interaction with FtsA on the membrane. The chiral organization of FtsZ filaments is analogous to chiral filaments of MreB *in vivo*[55], which were suggested to give rise to chiral ordering of the cell wall during cell elongation. Our findings support the view of the Z-ring continuously adapting to the decreasing diameter of the constricting division septum. A highly dynamic Z-ring could act as a scaffold to spatially organize the enzymes required for the inward growth of the cell wall. In this case, the mechanical force would primarily arise from bond formation during cell wall biosynthesis, as described for MreB (refs 56,57), before the Z-ring itself performs the final scission event[24]. □

METHODS

Methods and any associated references are available in the online version of the paper.

Note: Supplementary Information is available in the online version of the paper

ACKNOWLEDGEMENTS

We thank the members of the laboratories of T.J.M., T. Bernhardt and T. Rapoport for discussions and support; J. Werbin (Harvard Medical School, USA) for the plasmid for sortase expression; H. Erickson (Duke University, USA) for the plasmid for FtsZ–YFP–mts expression; J. Brugues for valuable discussions and advice; and E. Garner, K. Kruse and S. Grill for discussions and comments on the manuscript. We would also like to thank the Nikon Imaging Center at Harvard Medical School for their excellent service. M.L. is supported by fellowships from EMBO (ALTF 394-2011) and HFSP (LT000466/2012). Cytoskeleton dynamics research in the T.J.M. group is supported by NIH-GM39565.

AUTHOR CONTRIBUTIONS

M.L. designed and performed experiments and analysed results. M.L. and T.J.M. discussed results and wrote the paper.

COMPETING FINANCIAL INTERESTS
The authors declare no competing financial interests.

Published online at www.nature.com/doifinder/10.1038/ncb2885
Reprints and permissions information is available online at www.nature.com/reprints

1. Cabeen, M. T. & Jacobs-Wagner, C. The bacterial cytoskeleton. *Annu. Rev. Genet.* **44,** 365–392 (2010).
2. Ingerson-Mahar, M. & Gitai, Z. A growing family: the expanding universe of the bacterial cytoskeleton. *FEMS Microbiol. Rev.* **36,** 256–266 (2012).
3. Margolin, W. FtsZ and the division of prokaryotic cells and organelles. *Nat. Rev. Mol. Cell Biol.* **6,** 862–871 (2005).
4. Adams, D. W. & Errington, J. Bacterial cell division: assembly, maintenance and disassembly of the Z ring. *Nat. Rev. Microbiol.* **7,** 642–653 (2009).
5. Erickson, H. P., Taylor, D. W., Taylor, K. A. & Bramhill, D. Bacterial cell division protein FtsZ assembles into protofilament sheets and minirings, structural homologs of tubulin polymers. *Proc. Natl Acad. Sci. USA* **93,** 519–523 (1996).
6. Lu, C., Reedy, M. & Erickson, H. Straight and curved conformations of FtsZ Are regulated by GTP hydrolysis. *J. Bacteriol.* **182,** 164–170 (2000).
7. Oliva, M. A., Trambaiolo, D. & Löwe, J. Structural insights into the conformational variability of FtsZ. *J. Mol. Biol.* **373,** 1229–1242 (2007).
8. Hsin, J., Gopinathan, A. & Huang, K. C. Nucleotide-dependent conformations of FtsZ dimers and force generation observed through molecular dynamics simulations. *Proc. Natl Acad. Sci. USA* **109,** 9432–9437 (2012).
9. Pichoff, S. & Lutkenhaus, J. Unique and overlapping roles for ZipA and FtsA in septal ring assembly in *Escherichia coli*. *EMBO J.* **21,** 685–693 (2002).
10. Pichoff, S. & Lutkenhaus, J. Tethering the Z ring to the membrane through a conserved membrane targeting sequence in FtsA. *Mol. Microbiol.* **55,** 1722–1734 (2005).
11. Beuria, T. K. *et al.* Adenine nucleotide-dependent regulation of assembly of bacterial tubulin-like FtsZ by a hypermorph of bacterial actin-like FtsA. *J. Biol. Chem.* **284,** 14079–14086 (2009).
12. Szwedziak, P., Wang, Q., Freund, S. M. & Löwe, J. FtsA forms actin-like protofilaments. *EMBO J.* **31,** 2249–2260 (2012).
13. Hale, C. A. & de Boer, P. A. J. Direct binding of FtsZ to ZipA, an essential component of the septal ring structure that mediates cell division in *E. coli*. *Cell* **88,** 175–185 (1997).
14. Liu, Z., Mukherjee, A. & Lutkenhaus, J. Recruitment of ZipA to the division site by interaction with FtsZ. *Mol. Microbiol.* **31,** 1853–1861 (1999).
15. Mosyak, L. *et al.* The bacterial cell-division protein ZipA and its interaction with an FtsZ fragment revealed by X-ray crystallography. *EMBO J.* **19,** 3179–3191 (2000).
16. Ma, X. & Margolin, W. Genetic and functional analyses of the conserved C-terminal core domain of *Escherichia coli* FtsZ. *J. Bacteriol.* **181,** 7531–7544 (1999).
17. Haney, S. A. *et al.* Genetic analysis of the *Escherichia coli* FtsZ.ZipA interaction in the yeast two-hybrid system. Characterization of FtsZ residues essential for the interactions with ZipA and with FtsA. *J. Biol. Chem.* **276,** 11980–11987 (2001).
18. Erickson, H. P. & Osawa, M. Cell division without FtsZ—a variety of redundant mechanisms. *Mol. Microbiol.* **78,** 267–270 (2010).
19. Kirkpatrick, C. L. & Viollier, P. H. New(s) to the (Z-)ring. *Curr. Opin. Microbiol.* **14,** 691–697 (2011).
20. Lutkenhaus, J., Pichoff, S. & Du, S. Bacterial cytokinesis: from Z ring to divisome. *Cytoskeleton (Hoboken)* **69,** 778–790 (2012).
21. Osawa, M., Anderson, D. E. & Erickson, H. P. Reconstitution of contractile FtsZ rings in liposomes. *Science* **320,** 792–794 (2008).
22. Osawa, M., Anderson, D. E. & Erickson, H. P. Curved FtsZ protofilaments generate bending forces on liposome membranes. *EMBO J.* **28,** 3476–3484 (2009).
23. Arumugam, S. *et al.* Surface topology engineering of membranes for the mechanical investigation of the tubulin homologue FtsZ. *Angew. Chem. Int. Ed. Engl.* **51,** 11858–11862 (2012).
24. Osawa, M. & Erickson, H. P. Liposome division by a simple bacterial division machinery. *Proc. Natl Acad. Sci. USA* **110,** 11000–11004 (2013).
25. Uehara, T., Parzych, K. R., Dinh, T. & Bernhardt, T. G. Daughter cell separation is controlled by cytokinetic ring-activated cell wall hydrolysis. *EMBO J.* **29,** 1412–1422 (2010).
26. Rueda, S., Vicente, M. & Mingorance, J. Concentration and assembly of the division ring proteins FtsZ, FtsA, and ZipA during the *Escherichia coli* cell cycle. *J. Bacteriol.* **185,** 3344–3351 (2003).
27. Moran, U., Phillips, R. & Milo, R. SnapShot: key numbers in biology. *Cell* **141,** 1262.e1 (2010).
28. Thanedar, S. & Margolin, W. FtsZ exhibits rapid movement and oscillation waves in helix-like patterns in *Escherichia coli*. *Curr. Biol.* **14,** 1167–1173 (2004).
29. Ben-Yehuda, S. & Losick, R. Asymmetric cell division in *B. subtilis* involves a spiral-like intermediate of the cytokinetic protein FtsZ. *Cell* **109,** 257–266 (2002).
30. Martos, A. *et al.* Isolation, characterization and lipid-binding properties of the recalcitrant FtsA division protein from *Escherichia coli*. *PLoS ONE* **7,** e39829 (2012).
31. Pichoff, S. & Lutkenhaus, J. Identification of a region of FtsA required for interaction with FtsZ. *Mol. Microbiol.* **64,** 1129–1138 (2007).
32. Pichoff, S., Shen, B., Sullivan, B. & Lutkenhaus, J. FtsA mutants impaired for self-interaction bypass ZipA suggesting a model in which FtsA's self-interaction competes with its ability to recruit downstream division proteins. *Mol. Microbiol.* **83,** 151–167 (2011).
33. Li, Z., Trimble, M. J., Brun, Y. V. & Jensen, G. J. The structure of FtsZ filaments *in vivo* suggests a force-generating role in cell division. *EMBO J.* **26,** 4694–4708 (2007).
34. Niu, L. & Yu, J. Investigating intracellular dynamics of FtsZ cytoskeleton with photoactivation single-molecule tracking. *Biophys. J.* **95,** 2009–2016 (2008).
35. Lan, G., Daniels, B. R., Dobrowsky, T. M., Wirtz, D. & Sun, S. X. Condensation of FtsZ filaments can drive bacterial cell division. *Proc. Natl Acad. Sci. USA* **106,** 121–126 (2009).
36. Needleman, D. J. *et al.* Fast microtubule dynamics in meiotic spindles measured by single molecule imaging: evidence that the spindle environment does not stabilize microtubules. *Mol. Biol. Cell* **21,** 323–333 (2010).
37. Chen, Y. & Erickson, H. P. Rapid in vitro assembly dynamics and subunit turnover of FtsZ demonstrated by fluorescence resonance energy transfer. *J. Biol. Chem.* **280,** 22549–22554 (2005).
38. Mingorance, J. *et al.* Visualization of single Escherichia coli FtsZ filament dynamics with atomic force microscopy. *J. Biol. Chem.* **280,** 20909–20914 (2005).
39. Mateos-Gil, P. *et al.* Depolymerization dynamics of individual filaments of bacterial cytoskeletal protein FtsZ. *Proc. Natl Acad. Sci. USA* **109,** 8133–8138 (2012).
40. Hale, C. A., Rhee, A. C. & de Boer, P. A. ZipA-induced bundling of FtsZ polymers mediated by an interaction between C-terminal domains. *J. Bacteriol.* **182,** 5153–5166 (2000).
41. Hernandez-Rocamora, V. M. *et al.* Dynamic interaction of the Escherichia coli cell division ZipA and FtsZ proteins evidenced in nanodiscs. *J. Biol. Chem.* **287,** 30097–30104 (2012).
42. Mateos-Gil, P. *et al.* FtsZ polymers bound to lipid bilayers through ZipA form dynamic two dimensional networks. *Biochim. Biophys. Acta* **1818,** 806–813 (2012).
43. Martos, A. *et al.* Characterization of self-association and heteroassociation of bacterial cell division proteins FtsZ and ZipA in solution by composition gradient-static light scattering. *Biochemistry* **49,** 10780–10787 (2010).
44. Tyson, J. J., Chen, K. C. & Novák, B. Sniffers, buzzers, toggles and blinkers: dynamics of regulatory and signaling pathways in the cell. *Curr. Opinion Cell Biol.* **15,** 221–231 (2003).
45. Alon, U. Network motifs: theory and experimental approaches. *Nat. Rev. Genet.* **8,** 450–461 (2007).
46. Novák, B. & Tyson, J. J. Design principles of biochemical oscillators. *Nat. Rev. Mol. Cell Biol.* **9,** 981–991 (2008).
47. Lange, G., Mandelkow, E. M., Jagla, A. & Mandelkow, E. Tubulin oligomers and microtubule oscillations. Antagonistic role of microtubule stabilizers and destabilizers. *Eur. J. Biochem.* **178,** 61–69 (1988).
48. Henley, C. L. Possible origins of macroscopic left-right asymmetry in organisms. *J. Stat. Phys.* **148,** 740–774 (2012).
49. Nédélec, F. J., Surrey, T., Maggs, A. C. & Leibler, S. Self-organization of microtubules and motors. *Nature* **389,** 305–308 (1997).
50. Schaller, V., Weber, C., Semmrich, C., Frey, E. & Bausch, A. R. Polar patterns of driven filaments. *Nature* **467,** 73–77 (2010).
51. Sumino, Y. *et al.* Large-scale vortex lattice emerging from collectively moving microtubules. *Nature* **483,** 448–452 (2012).
52. Sanchez, T., Chen, D. T. N., DeCamp, S. J., Heymann, M. & Dogic, Z. Spontaneous motion in hierarchically assembled active matter. *Nature* **491,** 431–434 (2012).
53. Hitt, A. L., Cross, A. R. & Williams, R. C. Microtubule solutions display nematic liquid crystalline structure. *J. Biol. Chem.* **265,** 1639–1647 (1990).
54. Käs, J. *et al.* F-actin, a model polymer for semiflexible chains in dilute, semidilute, and liquid crystalline solutions. *Biophys. J.* **70,** 609–625 (1996).
55. Wang, S., Furchtgott, L., Huang, K. C. & Shaevitz, J. W. Helical insertion of peptidoglycan produces chiral ordering of the bacterial cell wall. *Proc. Natl Acad. Sci. USA* **109,** E595–E604 (2012).
56. Garner, E. C. *et al.* Coupled, circumferential motions of the cell wall synthesis machinery and MreB filaments in *B. subtilis*. *Science* **333,** 222–225 (2011).
57. Domínguez-Escobar, J. *et al.* Processive movement of MreB-associated cell wall biosynthetic complexes in bacteria. *Science* **333,** 225–228 (2011).

METHODS

Protein biochemistry. Untagged FtsZ was purified as a His–SUMO fusion from pTB567. As FtsZ does not contain a native cysteine, we modified FtsZ with an amino-terminal cysteine residue (Cys-FtsZ) by introducing seven additional amino acids (AEGCGEL) to the N terminus of the protein to obtain pT567–GCG-FtsZ (both plasmids were gifts from T. Bernhardt, Harvard Medical School, USA). Both versions of FtsZ were expressed in C41 cells grown in 2XYT medium at 37 °C and incubated to an attenuance of 0.8 at 600 nm. Expression was induced by adding IPTG to 1 mM and growing the cells at 37 °C for 5 h. The collected cells were pelleted and resuspended in lysis buffer (50 mM Tris-HCl at pH 8.0, 50 mM KCl, 20 mM imidazole, 10% glycerol, 10 mM β-mercaptoethanol and protease inhibitor (Complete EDTA free, Roche Molecular Biochemicals)) and stored at −80 °C. For purification, cells were thawed, incubated with lysozyme (10 mg ml^{-1}, L-6876, Sigma-Aldrich) and DNase (1 mg ml^{-1}, DN25, Sigma-Aldrich) and lysed by sonification. The resulting extract was centrifuged at 45,000*g* for 20 min at 4 °C to pellet cell debris and membranes. The clarified lysate was then loaded onto a Ni^{2+} agarose column (HisPur Ni-NTA resin, Thermo Scientific). The column was washed with lysis and wash buffer (50 mM Tris-HCl at pH 8.0, 50 mM KCl, 30 mM imidazole, 10% glycerol, 10 mM β-mercaptoethanol and protease inhibitors (Complete, Roche)) and eluted with elution buffer (50 mM Tris-HCl at pH 8.0, 50 mM KCl, 200 mM imidazole, 10% glycerol and 10 mM β-mercaptoethanol). Peak His–Sumo–FtsZ fractions were pooled. The H-SUMO tag was cleaved with 6xHis-tagged SUMO protease during dialysis into 50 mM Tris, at pH 8.0, 300 mM KCl and 10% glycerol. The protease and released tag were removed from the preparation by passing it over Ni-NTA resin. After removal of the tag, Cys-FtsZ was labelled by thiol-reactive dyes (Alexa488–maleimide, Molecular Probes; Cy5–maleimide, GE Healthcare) according to the protocols of the manufacturer. Polymerization-competent proteins were enriched by $CaCl_2$-mediated polymerization. The FtsZ preparation was dialysed against FtsZ polymerization buffer (50 mM piperazine-*N*,*N*′-bis(2-ethanesulphonic acid), at pH 6.7, and 10 mM $MgCl_2$) and warmed to room temperature. $CaCl_2$ and GTP were added to the final concentrations of 10 mM and 5 mM, respectively, and the reaction was centrifuged at 20,000*g* for 2 min at room temperature to pellet polymeric FtsZ. FtsZ pellets were resuspended in storage buffer (50 mM Tris, at pH 7.4, 50 mM KCl, 1 mM EDTA and 10% glycerol) and dialysed extensively to remove $CaCl_2$ and free GTP.

FtsA was PCR-amplified from MG1655 cells and cloned into pTB146 (a gift from T. Bernhardt (Harvard Medical School, USA)) restriction-digested with SapI and XhoI to obtain pML29. For labelling of FtsA we introduced a pentaglycine tag (Gly5–FtsA) at the N terminus of FtsA to obtain pML60. Both versions of FtsA were expressed as a His–SUMO fusion in C41 cells grown in 2XYT medium at 37 °C and incubated to an attenuance of 1–1.5 at 600 nm. The SUMO construct allowed for increased solubility of the protein and decreased toxicity for the cells. Expression was induced by adding IPTG to 1 mM and growing the cells at 18 °C overnight. Collected cells were resuspended in lysis buffer (50 mM Tris-HCl at pH 8, 20 mM imidazol, 500 mM NaCl, 10 mM $MgCl_2$, 10 mM β-mercaptoethanol, 1 mM ADP and protease inhibitors). After lysis, the lysate was loaded onto a Ni^{2+} agarose column, which was washed with wash buffer (50 mM Tris-HCl at pH 8, 500 mM KCl, 30 mM imidazol, 10 mM $MgCl_2$, 10 mM β-mercaptoethanol and 1 mM ADP). His–SUMO–FtsA was eluted at 200 mM imidazol and peak protein fractions were pooled. The SUMO tag was removed by adding Ulp1 to 5 mM and incubation on ice for 3.5 h. The protease and released tag were removed from the untagged FtsA by gel filtration using a Superdex 200 column and FtsA storage buffer (50 mM HEPES at pH 7.55, 500 mM KCl, 10 mM $MgCl_2$, 10% glycerol and 1 mM ADP). Peak fractions of FtsA were pooled and concentrated to 50 μM, flash frozen in liquid nitrogen and stored at −80 °C. FtsZ was fluorescently labelled by 'sortagging'[58]: His–SUMO–Gly5–FtsA was incubated with 5 mM Ulp1 and additionally 50 μM His–SrtΔ59 in the presence of 1 mM Cy5-labelled pentapeptide LPTEG and 5 mM $CaCl_2$. The protease, sortase, tag and excess Cy5-pentapeptide were removed by gel filtration to obtain Cy5–GG-FtsA. Mutants of FtsA were obtained by site-directed mutagenesis (Quikchange, Agilent).

Mutants of FtsA were obtained by site-directed mutagenesis (Quikchange, Stratagene) following the instructions of the manufacturer to obtain pML35, pML52 and pML53.

ZipA without the N-terminal periplasmic and transmembrane domains, that is, amino acids 23–328, was cloned into pET28a to obtain pML21 and purified as His–Δ22-ZipA fusion. Truncated ZipA was expressed in C41 cells grown in 2XYT medium at 37 °C and incubated to an attenuance of 0.8 at 600 nm. Expression was induced by adding IPTG to 1 mM and growing the cells at 37 °C for another 3 h. The protein was purified using a Ni^{2+} agarose column (HisPur Ni-NTA resin, Thermo Scientific). Purity of the proteins was confirmed by SDS–PAGE stained with Coomassie blue (Supplementary Fig. 1). His–SrtΔ59, His–Ulp1 and FtsZ–YFP–mts were purified according to previously published protocols[21,59,60].

All plasmids were verified by DNA sequencing. Oligonucleotide primers used in these study are given in Supplementary Table 2.

Preparation of liposomes. *E. coli* polar lipids dissolved in chloroform were transferred into a glass vial and the solvent was evaporated under a gentle stream of nitrogen. Any residual solvent was further removed by drying the lipid film in a vacuum for 1 h. The lipids were then rehydrated in SLB buffer (50 mM Tris at pH 7.5, 300 mM KCl and 5 mM $MgCl_2$) to a lipid concentration of 4 mg ml^{-1} and incubated at 37 °C for 30 min. The lipid film was then completely resuspended by vortexing rigorously to obtain multilamellar vesicles of different sizes. This mixture was then placed in a bath sonicator where shear forces help to reduce the size of the vesicles, giving rise to small unilamellar vesicles (SUVs). This SUV dispersion was stored at −20 °C as 20 μl aliquots.

Vesicle sedimentation assay. Liposomes were prepared as described above in 50 mM PIPES at pH 6.7, 50 mM KCl and 10 mM $MgCl_2$, and sonicated only briefly to obtain multilamellar vesicles of different sizes. Purified proteins (5 μM FtsZ, 3 μM FtsA or 3 μM ZipA) were added to a suspension of 2 mg ml^{-1} SUVs in reaction buffer. Reactions were started by adding GTP (and in the case of FtsA with, additionally, ATP) to 1 mM and incubated at room temperature for 10 min. Vesicles were sedimented by centrifugation at 25 000 r.p.m. in a Beckmann TLA-100 rotor in a table-top ultracentrifuge at room temperature for 10 min. The supernatant of each mixture was collected and the pellet was resuspended in reaction buffer to the original volume. Amounts of FtsZ, FtsA or ZipA were estimated by SDS–PAGE. Following electrophoresis, gels were stained with Coomassie blue.

Preparation of supported lipid bilayers. Glass coverslips were cleaned by sonicating in 2% Hellmanex II solution (Hellma) for 15 min, followed by extensive washing with milliQ H_2O. Finally, glass coverslips were washed, sonicated and stored in 95% reagent-grade ethanol. Before use, glass coverslips were blown dry with compressed air and cleaned in an air plasma for 15 min. The reaction chamber for the self-organization assay was prepared by attaching a plastic ring on a cleaned glass coverslip using ultraviolet glue (Norland optical adhesive 88). For supported lipid bilayer formation, the SUV dispersion was diluted in SLB buffer to 0.5 mg ml^{-1}, of which 75 μlwas added to the reaction chamber. Adding $CaCl_2$ to a final concentration of 3 mM induced fusion of the vesicles and the formation of a lipid bilayer on the mica surface. After 10 min of incubation at 37 °C, the sample was rinsed with 2 ml pre-warmed reaction buffer.

FtsZ self-organization assay. For the self-organization assay of FtsZ and FtsA, FtsZ with 30% Alexa488-labelled FtsZ, FtsA with optionally 30% Cy5–GG-FtsA at different concentrations and ATP (1 mM) were added to the reaction buffer (50 mM Tris-HCl at pH 7.5, 150 mM KCl and 5 mM $MgCl_2$) above the supported lipid membrane in a self-made reaction chamber (Supplementary Fig. 1). The final volume of the assay was 100 μl. The reaction chamber was closed with a lid of an Eppendorf reaction tube during observation. Polymerization of FtsZ was induced by adding GTP to 2.5 mM to the buffer, which allowed polymerization for about 2 h. For experiments on FtsZ and ZipA, we first added His–ZipA (1 μM) to the buffer and allowed it to bind to bilayers containing 4% 18:1 DGS-NTA (Ni^{2+}). After 10 min, we washed the system four times with 200 μl reaction buffer to remove unbound protein, before we added FtsZ to the buffer. All experiments were performed with an oxygen scavenger system (40 mM D-glucose, 0.040 mg ml^{-1} glucose oxidase, 0.016 mg ml^{-1} catalase, 20 mM dithiothreitol and 1 mM trolox) added to the buffer to prevent photobleaching.

Total internal reflection fluorescence microscopy imaging. All experiments were performed on a Nikon Ti total internal reflection fluorescence microscope equipped with a ×100 total internal reflection fluorescence NA 1.49 differential interference contrast objective lens and the Perfect Focus System for continuous maintenance of focus. Alexa488 was excited with a 100 mW 491 nm solid-state laser of Solamere laser launch, Cy5 with a 30 mW 640 nm laser. The laser line was selected using a fibre-optic delivery system and 4-channel acousto-optic tunable filter. Images were acquired with a Hamamatsu ImagEM 512x512 back-thinned electron-multiplying cooled CCD (charge-coupled device) camera controlled with Nikon Elements software. For time-lapse experiments, images were obtained every 2–5 s, with 30 ms exposure time, with illumination light shuttered between acquisitions.

Single-particle tracking. Tracking of individual FtsZ monomers was performed as described in ref. 61. During each experiment, 5–10 videos were acquired. For each video (between 200 and 500 frames with a total run length of 50–160 s), a minimum number of 100 protein tracks were analysed. Therefore, one experimental value represents the average of at least 500 analysed particles. The averaged value of five exper-

DOI: 10.1038/ncb2885

iments represents at least 1,500 analysed tracks. At the imaging conditions we used, we found that the observed number of fluorescent molecules did not decrease with observation time, suggesting that the bleaching time was longer than the lifetime of FtsZ on the membrane. As a further control, we decreased the frame rate during data acquisition, such that the time between two successive frames increased from 0.5 s and 0.8 s and we did not see a significant difference in the observed lifetimes, indicating that bleaching occurred on a longer timescale than the binding/unbinding events and that it did not contribute significantly to the measured lifetimes.

Image analysis and processing. Image analysis and processing was carried out with ImageJ (Rasband, W. S., ImageJ, US National Institutes of Health, Bethesda, http://rsb.info.nih.gov/ij/, 1997–2007). The frames of time-lapse movies were normalized to have a constant overall intensity, thus compensating for the increasing intensity over time due to protein binding to the membrane. As a consequence of this normalization, nonspecific bound fluorescent particles appear disproportionately bright at the beginning of a movie. Kymographs of ring rotation were obtained using an ImageJ kymograph plugin from J. Rietdorf and A. Seitz (EMBL, Heidelberg; http://www.embl.de/eamnet/html/kymograph.html).

Repeatability of experiments. Representative micrographs and intensity curves correspond to at least four (up to more than 100) successfully repeated experiments. The number of replicated experiments is given in the respective figure captions. For the analysis of single FtsZ filaments (Fig. 2d and Supplementary Fig. 3), we selected 38 isolated filaments, whose trajectories did not cross with those of neighbouring filaments as resolved in our microscopic set-up.

58. Popp, M. W., Antos, J. M., Grotenbreg, G. M., Spooner, E. & Ploegh, H. L. Sortagging: a versatile method for protein labeling. *Nat. Chem. Biol.* **3,** 707–708 (2007).
59. Popp, M. W-L., Antos, J. M. & Ploegh, H. L. Site-specific protein labeling via sortase-mediated transpeptidation. *Curr. Protoc. Protein Sci.* **56,** 15.3.1.–15.3.9. (2009).
60. Mossessova, E. & Lima, C. D. Ulp1-SUMO crystal structure and genetic analysis reveal conserved interactions and a regulatory element essential for cell growth in yeast. *Mol. Cell* **5,** 865–876 (2000).
61. Loose, M., Fischer-Friedrich, E., Herold, C., Kruse, K. & Schwille, P. Min protein patterns emerge from rapid rebinding and membrane interaction of MinE. *Nat. Struct. Mol. Biol.* **18,** 577–584 (2011).

DOI: 10.1038/ncb2885

nature cell biology

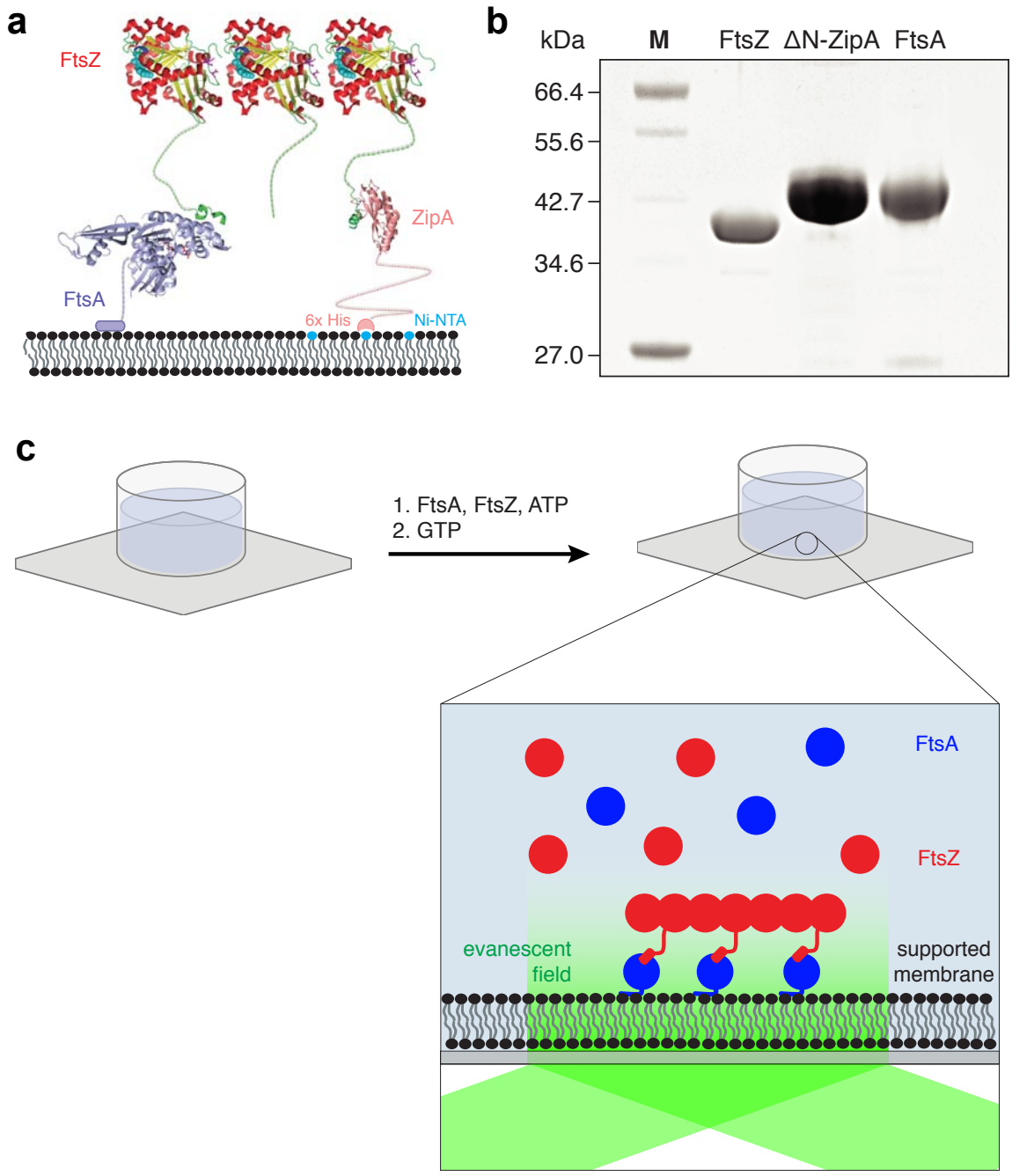

Supplementary Figure 1 Experimental assay. **(a)** Illustration of protein interactions lipids (adapted from ref. 20): FtsA and ZipA bind to same highly conserved C-tail of FtsZ (shown in green), which is connected to the rest of the protein by a flexible linker. FtsA binds to the membrane surface using an amphipathix helix, located at the end of a C-terminal flexible linker. ZipA is a transmembrane protein. The N-terminal transmembrane-domain has been substituted by a His-tag obtaining His-Δ22-ZipA, which was then permanently attached to the membrane using Ni^{2+}chelating. (**b**) Commassie-stained SDS-Page gel of purified proteins used for this study. (**c**) Schematic drawing of the experimental assay. A plastic ring was glued to a glass cover slip to create a reaction chamber and a supported lipid bilayer was formed on the glass surface. FtsA, FtsZ and ATP were added to the buffer before polymerization of FtsZ was initiated by adding GTP.

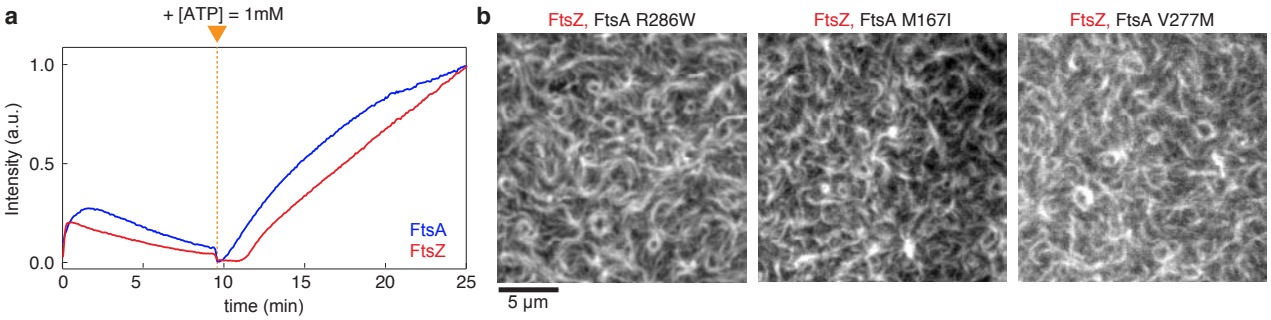

Supplementary Figure 2 Remodeling of cytoskeletal structures depends on the presence of ATP, but not on FtsA polymerization. (**a**) Representative intensity curve corresponding to Supplementary Video 4, showing the role of ATP for FtsZ-FtsA co-assembly: The initial transient binding of FtsZ to the membrane is likely due to residual amounts of ATP being co-purified with FtsA. After detachment of FtsZ and FtsA, the filament network reassembled as soon as fresh ATP is added (at orange arrowhead and dashed line). Similar intensity curves were obtained in 5 experiments. (**b**) FtsA polymerization is not important for the self-organization of FtsZ and FtsA in our *in vitro* system. When we used self-interaction mutants of FtsA (FtsA R286W (left), FtsA M167I (middle), FtsA V277M (right)), FtsZ formed the same cytoskeletal pattern as with the wildtype protein. Similar micrographs were obtained in n=10 experiments.

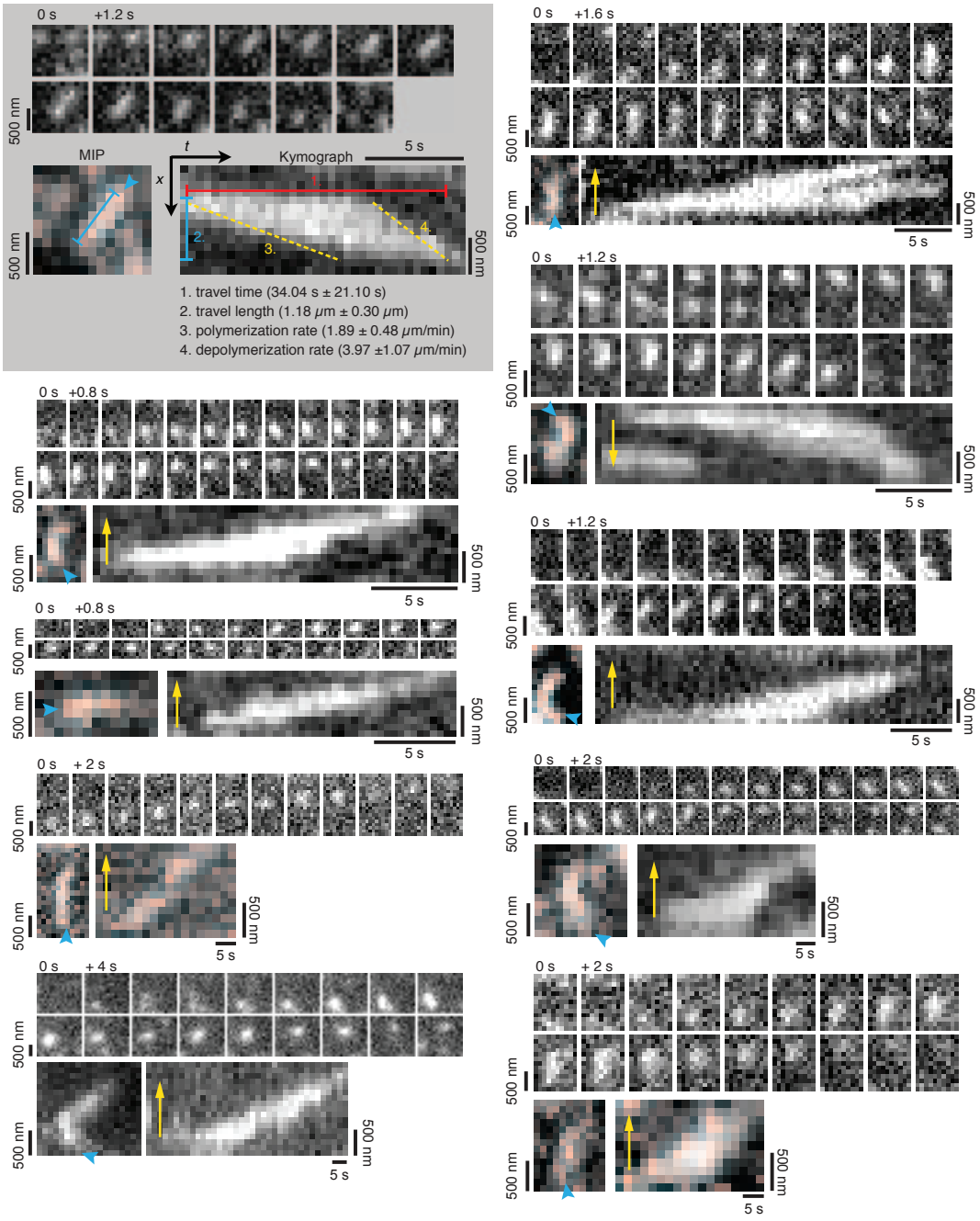

Supplementary Figure 3 Dynamics of single FtsZ filaments recruited to the membrane by FtsA. Snapshots, maximum intensity projections (MIP) and kymographs of single FtsZ filaments from movies acquired at a frame-rate of 2s or 400 ms (FtsZ = 0.45 μM with 30 mol-% FtsZ-Alexa488, FtsA = 0.2 μM). Cyan arrowheads in MIPs indicate the first binding of FtsZ to the membrane. Yellow arrows in kymograph show the polymerization direction. Top left, with grey background. Scale bars correspond to 500 nm or 5 s. Values in grey box (top left) represent average values of n=38 analyzed filaments from 5 independent experiments.

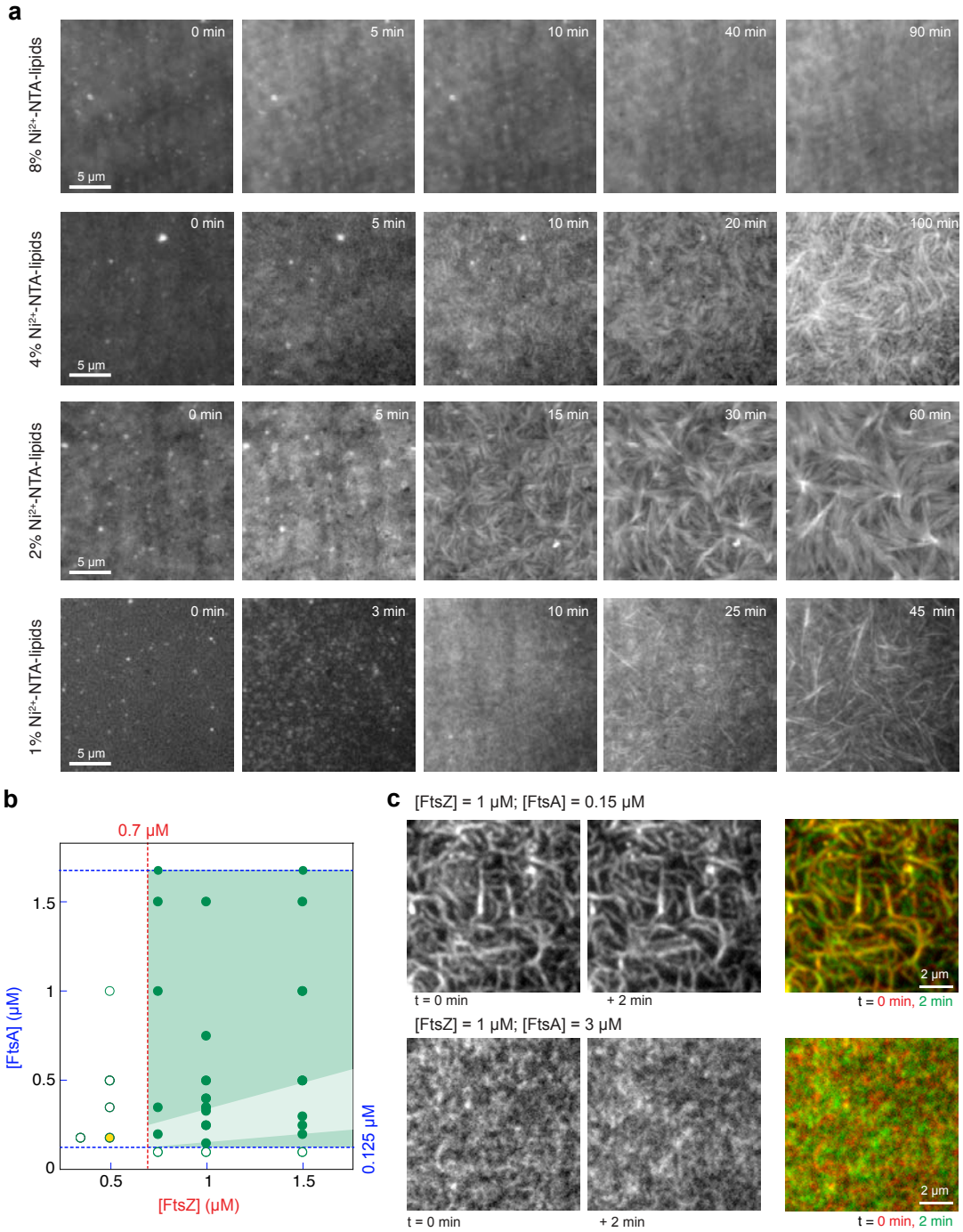

Supplementary Figure 4 Influence of different concentrations of membrane anchors on FtsZ filament patterns. (**a**) Representative snapshots of FtsZ filaments recruited to the membrane by ZipA at indicated time points after addition of GTP. The percentage of Ni^{2+}-chelating lipids (18:1 DGS-NTA-Ni^{2+}) defines the amount of ZipA immobilized and the amount of FtsZ recruited to the membrane. With 8% Ni^{2+}chelating lipids, FtsZ bundles densely covered the membrane. At lower concentrations (1%, 2% and 4%), bundles of FtsZ filaments start to appear after about 20 min. On membranes with 1% Ni^{2+}-chelating lipids, individual FtsZ filaments could briefly be resolved (see 3 min after addition of GTP), before the filament density became too high. Similar micrographs were obtained in 5 experiments. (**b**) Simplified phase diagram of FtsZ-FtsA filament networks on the membrane. Filled green dots represent experiments with protein concentrations allowing for the formation of a dynamic filament network (at protein concentrations of [FtsZ] > 0.7 µM and 0.125 µM < [FtsA] <1.7 µM). Empty dots represent experiments where FtsZ filaments were either too short for a continuous polymer network (with FtsZ < 0.7 µM) or where they did not show rapid rearrangements (with FtsA < 0.125 µM). Light green area represents the concentration ratio for FtsA and FtsZ found *in vivo*[26]. Yellow filled circle represents the concentration ratio used for single FtsZ filament experiments. (**c**) Representative snapshots and overlays of two individual frames separated by 2 min of a time-lapse movie. At low FtsA concentrations (top), FtsZ forms static, long filaments, whereas at high FtsA concentrations (bottom), filaments were short and dynamic, but did not form a continuous filament network. Similar micrographs were obtained in 5 experiments.

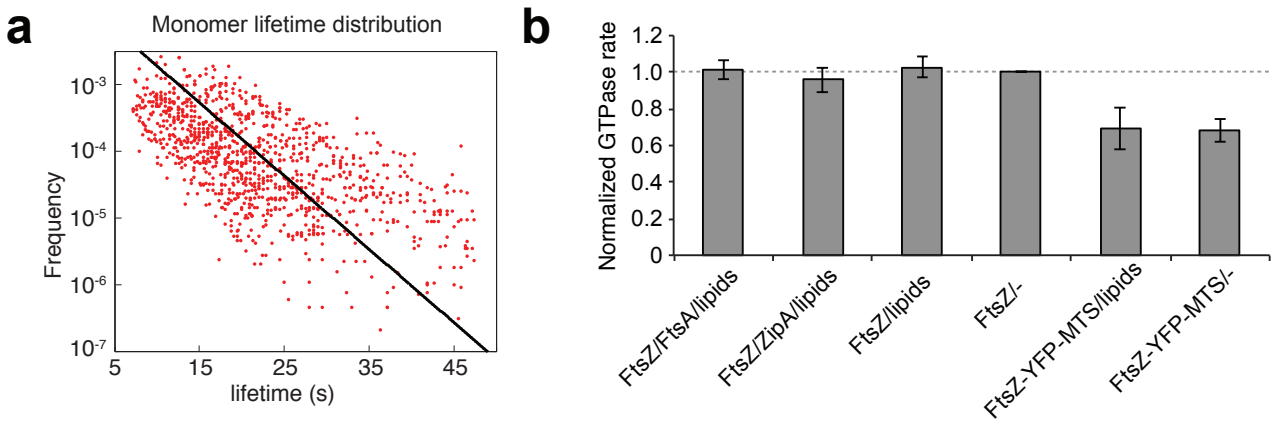

Supplementary Figure 5 The membrane anchor does not influence the GTPase rate and lifetime of FtsZ monomers. (**a**) With ZipA, the average lifetime of FtsZ was slightly longer than with FtsA. Linear-log plot of FtsZ lifetime distribution with ZipA as membrane anchor (filled red circles) about 30 min after addition of GTP. Black line represents the averaged linear fit to individual lifetime distributions with $<t> = 10.68\ s \pm 2.33\ s$ (s.d. n = 24 videos with 1500 particles obtained from 5 independent experiments), which is slightly longer than for FtsZ/FtsA (p=0.0174). (**b**) FtsZ GTPase activity was not affected by the membrane anchor. Bar graph shows GTPase activity of FtsZ (5 μM) or FtsZ-YFP-MTS (5 μM) and the influence of membrane anchors (His-ZipA or FtsA, 3 μM) and phospholipids (1 mg/ml). The corresponding rates were normalized to the GTP activity of FtsZ alone (0.083/s). We found that the GTPase activity of FtsZ-YFP-MTS to be about 30% lower than of wildtype FtsZ. GTPase activities were determined using the EnzChek Phosphate Assay Kit (Molecular Probes). Error bars correspond to s.d, from n=3 independent experiments.

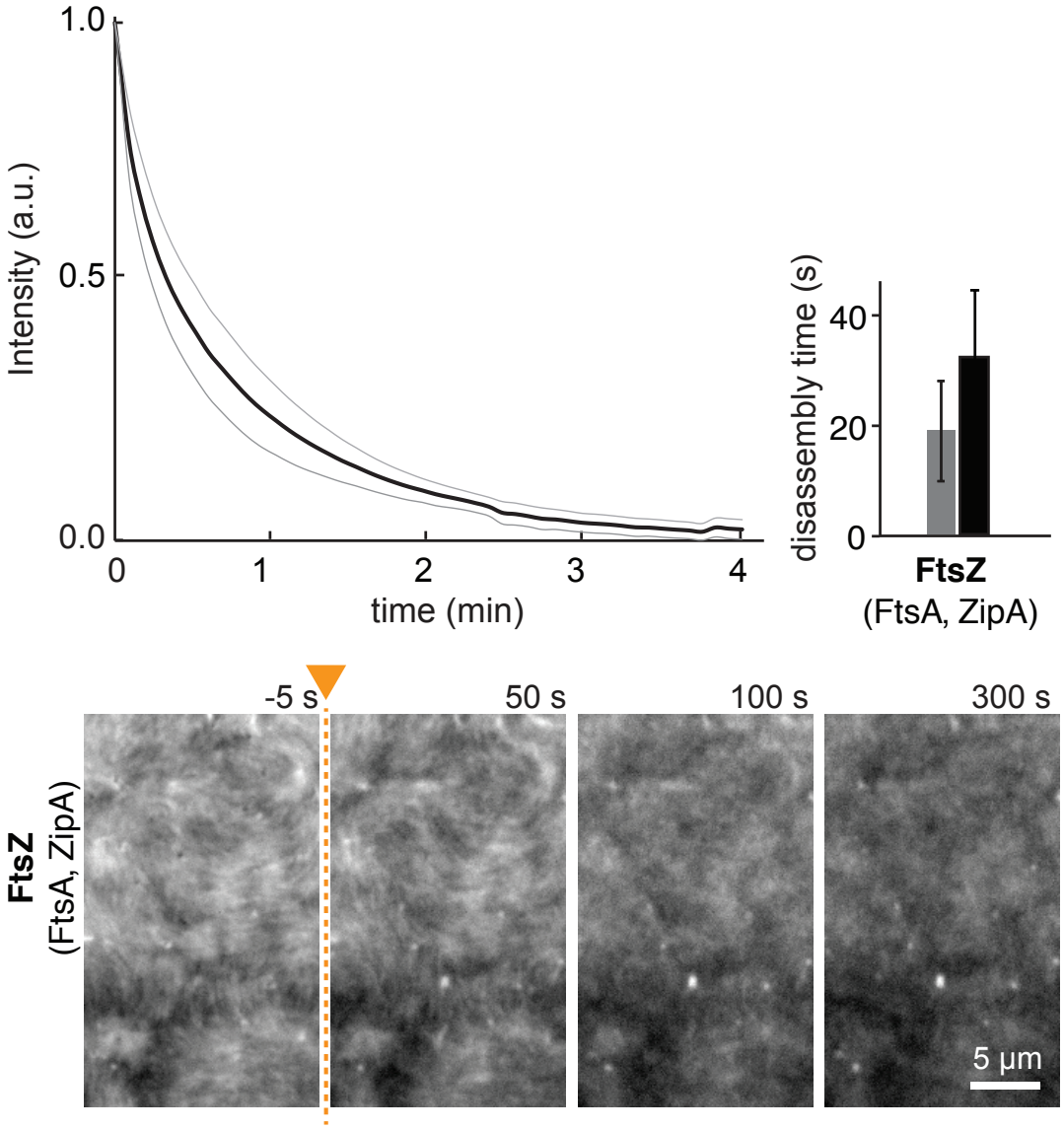

Supplementary Figure 6 FtsA destabilizes the FtsZ filament network also in presence of ZipA. Left, mean intensity traces for FtsZ depolymerization upon rapid dilution for FtsZ filaments recruited to the membrane by ZipA and FtsA. Right: mean disassembly times obtained from double-exponential fits, error bars and thin lines correspond to s.e.m, (n=3 independent experiments). Bottom: Representative snapshots showing disassembly of FtsZ filaments after dilution (time point of dilution is indicated by orange arrowhead and dashed line). In the presence of both anchors, ZipA and FtsA, no thick bundles of FtsZ persist on the membrane. Fluorescence intensity of each frame was normalized.

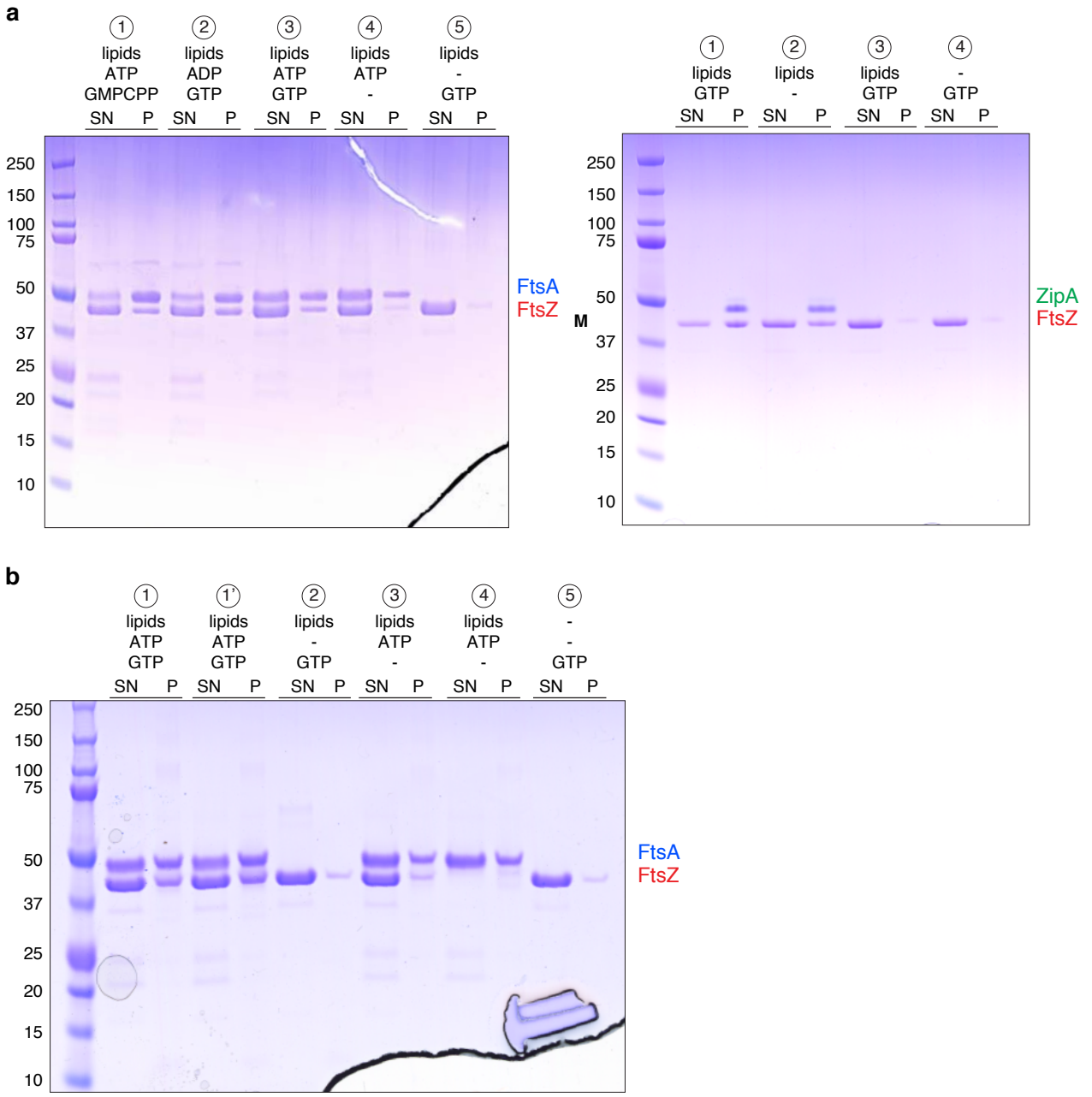

Supplementary Figure 7 Uncropped Commassie-stained SDS-Page gels corresponding to Figs. 3c (**a**) and 4d (**b**). P = Pellet, SN = Supernatant; 1 and 1' in **b** indicate replicates using identical experimental conditions.